

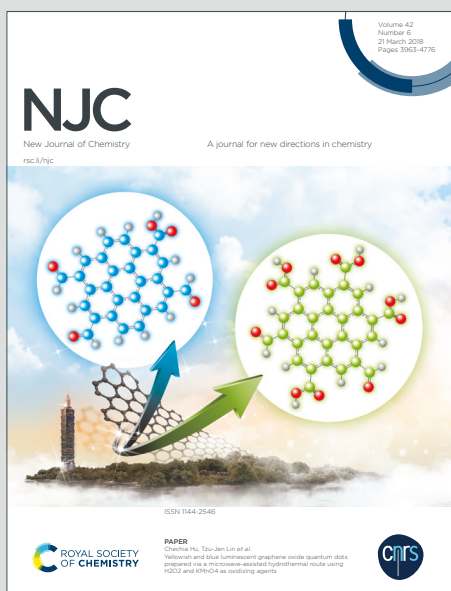
# NJC

New Journal of Chemistry

Accepted Manuscript

A journal for new directions in chemistry

This article can be cited before page numbers have been issued, to do this please use: C. Sepulveda, K. Cruces, J. Gajardo, J. Seguel, R. Garcia, D. Salinas, J. L. G. Fierro, I. T. Ghampson, R. Serpell and N. Escalona, *New J. Chem.*, 2019, DOI: 10.1039/C9NJ03534F.



This is an Accepted Manuscript, which has been through the Royal Society of Chemistry peer review process and has been accepted for publication.

Accepted Manuscripts are published online shortly after acceptance, before technical editing, formatting and proof reading. Using this free service, authors can make their results available to the community, in citable form, before we publish the edited article. We will replace this Accepted Manuscript with the edited and formatted Advance Article as soon as it is available.

You can find more information about Accepted Manuscripts in the [Information for Authors](#).

Please note that technical editing may introduce minor changes to the text and/or graphics, which may alter content. The journal's standard [Terms & Conditions](#) and the [Ethical guidelines](#) still apply. In no event shall the Royal Society of Chemistry be held responsible for any errors or omissions in this Accepted Manuscript or any consequences arising from the use of any information it contains.

## ARTICLE

## Promoter effect of Co on the catalytic activity of Cu oxide active phase supported on Al<sub>2</sub>O<sub>3</sub> in the hydrogenolysis of glycerol

C. Sepúlveda <sup>\*a,h</sup>, K. Cruces<sup>a,h</sup>, J. Gajardo<sup>a</sup>, J. Seguel<sup>a,h</sup>, R. García<sup>a</sup>, D. Salinas<sup>b\*\*</sup>, J. L. G. Fierro<sup>c</sup>, I. T. Ghampson<sup>d</sup>, R. Serpell<sup>e</sup>, N. Escalona <sup>f,g,h,i</sup>

Received 00th January 20xx,  
Accepted 00th January 20xx

DOI: 10.1039/x0xx00000x

The promoting effect of cobalt oxide on alumina-supported Cu oxide catalysts for the hydrogenolysis of glycerol was investigated. A series of Co(y)Cu/Al<sub>2</sub>O<sub>3</sub> oxide catalysts with a fixed Cu loading of 7 wt.% and a variable Co loading from 0 to 1.5wt.% was prepared by successive wet impregnation. The catalysts were characterized by X-ray diffraction (XRD), nitrogen sorption, temperature programmed reduction (TPR), ultraviolet-diffuse reflectance spectroscopy (UV-DRS), temperature programmed desorption of ammonia (TPD-NH<sub>3</sub>), and X-ray photoelectron spectroscopy (XPS). The catalysts were tested in a batch reactor at 220°C and 5 MPa of H<sub>2</sub>. The activity of the catalysts on a per mole of Cu basis increased with Co content up to plateau, and subsequently decreased at higher Co content. The increase of activity is attributed to the combined effect of the distortion of the octahedral geometry of CuO by the presence of CoO and the increase in the number of surface acid sites. In contrast, the subsequent decrease of activity at higher loading is related to formation of less reducible, less acidic, and less active aluminates. Products selectivity did not vary substantially with Co loading, indicative of the existence of active sites of similar characteristics on all the catalysts. Overall, all the catalysts favored the route comprising of C-O hydrogenolysis followed by hydrogenation, at the expense of the pathway involving C-C hydrogenolysis, leading to the predominant formation of 1,2-propanediol (1,2-PDO). This is probably due to the prevalence of metallic active sites over acidic sites on the surface, ensuring that partial removal of oxygen occurred without loss of carbon atoms.

### 1. Introduction

The production of biodiesel, considered an attractive alternative to crude oil, by transesterification of biomass-derived vegetable oils (triglycerides) has increased during the last decades. However, glycerol is obtained as a by-product during this process and constitutes about 10 wt.% of the total production, generating an annual accumulation of 1 million tons worldwide <sup>2</sup>, which is approximately 65% of the total glycerol produced <sup>3</sup>. Moreover, the purity of this compound is around of 80%, and the remaining 20% is heavily contaminated by free fatty acids, water, inorganic salts, unreacted triglycerides, methanol, among others <sup>3</sup>. These properties limit their direct use in certain applications and hinder their disposal as waste, requiring more sophisticated purification processes that ultimately raise the cost of biodiesel production and cause the closure of some industries. For this reason, the catalytic conversion of glycerol to produce a number of hydrocarbons, aldehydes and alcohols has been reported to be one of the most effective ways to address these issues. The conversion of glycerol to higher value-added products includes a series of selective processes, such as etherification, dehydration to acrolein, glycerol acid oxidation and hydrogenolysis to propanediols <sup>2, 4-6</sup>. The

selective hydrogenolysis of glycerol on bifunctional heterogeneous catalyst produces 1,2-propanediol (1,2-PDO), 1,3-propanediol (1,3-PDO), and ethyleneglycol (EG) <sup>7-9</sup>. In particular, the conversion of glycerol to 1,2-PDO has been extensively studied in order to understand the kinetic behavior and its mechanisms, since 1,2-PDO is an important raw material for the manufacture of polymers and pharmaceuticals, as well as for the production of liquid detergents, cosmetics, aromas and fragrances, personal care products, paints, animal feed, antifreeze, among others <sup>6</sup>.

Noble metals such as Ru, Rh and Pt have been widely used as catalysts for the hydrogenolysis of glycerol due to their high activity towards propanediols <sup>8, 10</sup>. However, due to the high cost of these metals non-noble metals that are active for hydrogenolysis reactions such as copper <sup>7, 9, 11, 12</sup>, nickel <sup>13-15</sup> and cobalt <sup>16, 17</sup> have received increased attention for glycerol conversion.

In particular, copper has been one of the most reported metallic catalysts for hydrogenolysis of glycerol due to its high hydrogenation activity <sup>12, 18</sup>, low activity towards C-C bond rupture, and high efficiency for the hydrogenation of C=O bonds to produce propanediols <sup>7, 9, 19</sup>. The last year the effect of Re as promoter of Cu and Ni supported catalysts in hydrogenolysis of glycerol have been study <sup>20, 21</sup>, showing an increase of selectivity to lower alcohols as methanol, ethanol and 1-propanol, by Re addition. Similar behavior in the same reaction was observed on Mo and W metal supported catalysts, but with major selectivity to lower alcohols in comparison to 1,2-PDO, it was attributed to an increase of Bronsted acid sites<sup>22</sup>. These researches indicated that Re, Mo and W metal active sites are no efficient to promoted the selectivity to 1,2-PDO, as a high added-value compound from hydrogenolysis of glycerol. Cobalt catalysts have received less attention but have been shown to be active in several hydrogenolysis reactions in which more than one C-C rupture is required <sup>16</sup>. Cobalt is also used industrially to promote dehydration and also for Fischer-Tropsch synthesis <sup>16</sup>.

<sup>a</sup> Universidad de Concepción, Facultad de Ciencias Químicas, Edmundo Larenas 129, Casilla 160C, Chile

<sup>b</sup> Universidad del Bio-Bio, Facultad de Ciencias, Departamento de Química, Avenida Collao 1202, Casilla 5C, Chile

<sup>c</sup> Instituto de Catálisis y Petroleoquímica, CSIC, Cantoblanco, 28049 Madrid, Spain.

<sup>d</sup> Department of Chemical System Engineering, The University of Tokyo, 7-3-1 Hongo, Bunkyo-ku, Tokyo 113-8656, Japan

<sup>e</sup> Departamento de Ingeniería y Gestión de la Construcción, Escuela de Ingeniería, Pontificia Universidad Católica de Chile, Santiago, Chile

<sup>f</sup> Departamento de Ingeniería Química y Bioprocesos, Escuela de Ingeniería, Pontificia Universidad Católica de Chile, Avenida Vicuña Mackenna 4860, Macul, Santiago, Chile.

<sup>g</sup> Facultad de Química y Farmacia, Pontificia Universidad Católica de Chile.

<sup>h</sup> Millennium Nuclei on Catalytic Processes Towards Sustainable Chemistry (CSC), Chile

<sup>i</sup> Unidad de Desarrollo Tecnológico, Universidad de Concepción, Coronel, Chile.

There is a continuing need to explore other active phases as part of concerted efforts towards developing effective catalysts for the conversion of glycerol to high value-added products.

One of the potential alternatives to metallic catalysts is metal oxide catalysts, particularly copper or cobalt oxide catalysts due to their propensity to cleave C-O bonds. Application of metal oxide catalysts also avoids the necessity to use hydrogen for catalyst pre-treatment. If partial metal reduction is required, the presence of H<sub>2</sub> in the reactant feed can potentially partially reduce surface oxides under experimental conditions. In addition, the oxygen vacancies created<sup>23, 24</sup> could provide adequate acidity on the surface<sup>25</sup> which could favor selectivity towards acetol, a precursor to 1,2-PDO<sup>19, 26</sup>. This acidity was on display when CuO/Al<sub>2</sub>O<sub>3</sub> catalysts were studied for dimethyl ether (DME) production via methanol dehydration: the results revealed that unbound CuO particles were dispersed on the surface of fresh CuO/Al<sub>2</sub>O<sub>3</sub> catalysts, providing the active sites for methanol decomposition<sup>27</sup>. In an unrelated study, Mao *et al.*<sup>28</sup> studied the catalytic hydrogenation of CO<sub>2</sub> to DME on CuO-ZnO-ZrO<sub>2</sub>/HZSM-5 catalysts and reported that the selectivity and yield to DME were directly related to CuO species, and that decrease of CO<sub>2</sub> adsorption capacity of the samples was related to the reducibility of CuO. These studies have demonstrated that reducible CuO active phase can catalyze hydrogenation routes and weaker acid sites formed on the surface favour dehydration reactions, both of which are key pathways during the hydrogenolysis of glycerol.

Critical catalyst parameters need to be investigated in order to assess the viability of reducible metal oxide active phase for glycerol hydrogenolysis. One of these parameters is the ability of a promoter to modify the acidity, nature and generation of active sites of metal oxide catalysts. According to reported by bibliography, Cu oxide is active for hydrogenation/dehydration reactions, and Co has been reported as a good promoter for several hydrogenation reactions. It should be pointed out that mixed copper-cobalt oxides have been applied in a variety of important catalytic reactions such as synthesis gas conversion to higher alcohols, carbon monoxide oxidation, reaction oxygen evolution (EOR), Fischer-Tropsch synthesis, among others. Mixed Cu-Co oxides have also been used in thermoelectric power generation materials<sup>29</sup>.

Therefore, considering the more efficiency C-O cleavage of Cu and Co in hydrotreatment reaction, compared to other transition metal catalysts, the aim of the current work is to provide insights into how Co oxide can improve the performance of CuO/Al<sub>2</sub>O<sub>3</sub> catalysts for the hydrogenolysis of glycerol. An investigation into the role of Co oxide in altering the reactivity of CuO active phase will lead to a greater understanding of the viability of this class of catalysts and provide useful guidance for their use for the hydrogenolysis of glycerol.

## Experimental

### 2.1 Catalyst preparation

The Co<sub>x</sub>(y)CuO/Al<sub>2</sub>O<sub>3</sub> catalysts, denoted as Co(y)Cu/Al<sub>2</sub>O<sub>3</sub>, were prepared by successive wetness impregnation using aqueous solution of Co(NO<sub>3</sub>)<sub>2</sub>·6H<sub>2</sub>O (Merck) and Cu(NO<sub>3</sub>)<sub>2</sub>·3H<sub>2</sub>O (Sigma Aldrich) as precursor salts and γ-Al<sub>2</sub>O<sub>3</sub> (SPH 50 LA) as support. Prior to impregnation, the support was crushed and sieved to 80 and 125 μm particle size. Aqueous solutions of different amounts of Co(NO<sub>3</sub>)<sub>2</sub>·6H<sub>2</sub>O, corresponding to Co nominal loadings of 0.8, 1.0, 1.3 and 1.5 wt.%, was first impregnated into the support, kept at room temperature for 24 h, dried at 120 °C for 12

h, and finally calcined at 300 °C for 2 h. Then, aqueous solution of Cu(NO<sub>3</sub>)<sub>2</sub>·3H<sub>2</sub>O, corresponding to 7 wt.% of Cu, was impregnated following the same procedure described, except that the samples were calcined at 500 °C for 2 h to obtain Co(y)Cu/Al<sub>2</sub>O<sub>3</sub> oxide catalysts. A monometallic Cu/Al<sub>2</sub>O<sub>3</sub> oxide catalyst was also prepared and used as reference following the same procedure and condition described for the impregnation of copper. The Cu and Co contents in the catalysts were determined by atomic absorption spectroscopy using a Thermo Scientific ICE 3000 model series, and are presented in Table 1.

### 2.2 Characterization of supports and catalysts

The BET specific surface area ( $S_{\text{BET}}$ ) and total pore volume ( $V_p$ ) of the catalysts and supports were determined from nitrogen sorption measurement at -196 °C using Micromeritics TriStar II 3020 equipment. Prior to the measurements, the samples were degassed at 300 °C for 2 h under vacuum. The BET specific surface area was calculated from the adsorption branch of the isotherms in the range  $0.05 \leq P/P^0 \leq 0.25$ , while the total pore volume was recorded at  $P/P^0 = 0.99$ .

Temperature programmed reduction (TPR) of the calcined sample was carried out in a quartz cell using a Micromeritics AutoChem II equipment equipped with a thermal conductivity detector. Approximately 20 mg of the sample was heated at 110 °C under He for 0.5 h, cooled to room temperature under He, and then heated under 5% H<sub>2</sub>/Ar (50 mLmin<sup>-1</sup>) from 25 °C to 1050 °C (10 °C min<sup>-1</sup>). The consumption of hydrogen was determined after internal calibration of the TCD.

XPS measurements were performed using a VG Escalab 200R electron spectrometer equipped with a hemispherical electron analyzer and Mg Kα (1253.6 eV) X-ray source. The samples were reduced *in-situ* at 400 °C under H<sub>2</sub> for 4h and transferred from the pre-treatment chamber to the spectrometer. The intensity of the peaks was estimated from the integral of each peak after subtracting an S-shaped background and fitting the curve to a combination of Gaussian/Lorentzian functions. Atomic ratios were calculated by using peak areas normalized on the basis of acquisition parameters, sensitivity and transmission factors provided by the manufacturer, and determined from the corresponding peak intensities, corrected with tabulated sensitivity factors, with a precision of ±7%.

Diffuse Reflectance UV-VIS (DRS) measurements of well-dried, calcined samples were carried out using a Lambda 35 spectrophotometer, equipped with a diffuse reflectance sphere for powder analysis. The UV-DR spectra were recorded in the wavelength range 200-900 nm at ambient conditions. The Kubelka-Munk's equation was used to calculate the intensities ( $I_{\text{OH}}/I_{\text{OHd}}$ ) ratio between Cu<sup>2+</sup> octahedral species ( $I_{\text{OH}}$ ) and octahedral distorted Cu<sup>2+</sup> species ( $I_{\text{OHd}}$ ) as a function of Co content.

Powder X-ray diffraction (XRD) patterns were obtained using a D4 Endeavor Bruker AXS diffractometer equipped with a nickel-filtered CuK<sub>α1</sub> radiation ( $\lambda = 1.5418 \text{ \AA}$ ). The standard scan parameters were 1° per min for the 2θ range from 10 to 90°. Identification of the phases was achieved by reference to ICDD files. In order to increase identification sensibility of the phases, the experimental patterns was performed using Match! software. Quantitative phase analysis was carried out using the Rietveld refinement of phase scale factors<sup>30</sup>. Prior to analysis of support materials, precursor material and catalyst samples, XRD equipment shape function and X-ray source parameters were refined using XRD data obtained from a pure corundum standard sample.

Temperature programmed desorption of ammonia (TPD-NH<sub>3</sub>) was performed using a TPR/TPD Micromeritics 2900 system equipped with a thermal conductivity detector (TCD). Prior to the analysis, the samples were dried under He (50 mL min<sup>-1</sup>) at 100 °C for 0.5 h. The TPD-NH<sub>3</sub> measurements were performed by pulsing NH<sub>3</sub> at 120 °C until saturation of the catalyst surface. Then, the samples were cooled to room temperature and purged under He to remove physically adsorbed NH<sub>3</sub>. Once the baseline was stabilized, the sample was heated to 700 °C by a ramp of 10 °C min<sup>-1</sup> under helium. The total amount of moles of desorbed ammonia in the samples (catalysts and supports) was obtained by the standardized DTP-ammonia analytical areas per catalyst mass. In addition, the semi-quantitative comparison of the distribution of acidic sites available on the surface was determined from the integration by Gaussian deconvolution of the ammonia desorption signals according to the temperature range at which the desorption signal appears; weak acid sites between 0-300 °C, moderate acid sites between 300-500 °C and strong acid sites at > 500 °C<sup>31</sup>.

### 2.3. Catalytic tests

Hydrogenolysis of glycerol was performed in a 300 mL batch reactor (4848 Parr model). The glycerol (> 99 % purity, Sigma Aldrich) concentration used was 10 mol L<sup>-1</sup> in deionized water. This concentration was selected after rigorous study of the optimal glycerol amount that needs to be used to avoid the high vapor pressure of water and the burning of glycerol. Similar high glycerol concentration has been reported by several authors<sup>32-34</sup>. Also, the mass of catalyst used has been experimentally verified to keep the reaction under kinetic regime without any diffusional limitations. In this context, the liquid reactant feed consisted of an aqueous glycerol solution (80 wt.%). About 0.5 g of oxide catalyst was added to the reactant. Then, the system was closed and N<sub>2</sub> was bubbled through the solution for 10 min to remove air from the system. Still under N<sub>2</sub>, the reactor was heated to the reaction temperature of 220 °C with continuous stirring. When this temperature was reached, H<sub>2</sub> was introduced into the reactor to 5 MPa which was kept constant during the course of the experiment. Condensed samples were taken periodically during the reaction and were identified and quantified using a Perkin Elmer Autosystem XL gas chromatograph with a flame ionization detector equipped with a capillary column (Nukol, 30 m x 0.53 mm x 0.5 μm).

The conversion of glycerol ( $X_{Gly}$ ) was calculated from:

$$X_{Gly}(\%) = \frac{n_{Gly}^0 - n_{Gly}^i}{n_{Gly}^0} \times 100 \quad (1)$$

where  $n_{Gly}^0$  is the initial moles of glycerol in the solution (mol) and  $n_{Gly}^i$  is the moles of glycerol at time  $i$  (mol). The specific rate for the total conversion of glycerol was calculated from the initial slope of the conversion vs. reaction time plot. The intrinsic rate was calculated from the specific rate according to the following equation:

$$r_i = r_s \frac{N}{nCu} \quad (2)$$

Where  $r_i$  is the intrinsic rate (molecules of glycerol converted per Cu atom per second),  $r_s$  is the specific rate (moles of glycerol converted per gram of catalyst per second),  $nCu$  represents the total number of Cu atoms per gram of catalyst, and  $N$  is Avogadro's number. The product distribution was calculated from Eq. (3) when the reaction was completed.

$$Selectivity(mol\%) = \frac{n_{productj}}{n_{Glyconverted}} \times 100 \quad (3)$$

Where  $n_{productj}$  is the moles of product  $j$  (mol) and  $n_{Glyconverted}$  is the moles of glycerol converted (mol).

## 2. Results and discussion

### 3.1 Catalysts and support Characterization

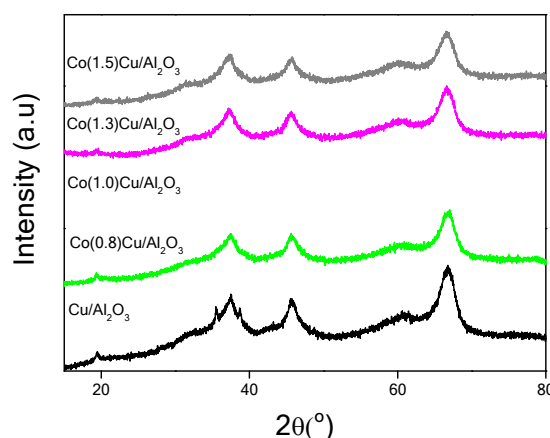
Table 1 summarizes the textural properties of the  $\gamma$ -Al<sub>2</sub>O<sub>3</sub> support, Cu/Al<sub>2</sub>O<sub>3</sub> and Co(y)Cu/Al<sub>2</sub>O<sub>3</sub> oxide catalysts. The BET surface area of the promoted Co(y)Cu/Al<sub>2</sub>O<sub>3</sub> oxide catalysts ranged from 213 to 225 m<sup>2</sup>g<sup>-1</sup>, which corresponds to a 29-33% decrease of  $S_{BET}$  of the support. The promoted catalysts presented similar specific surface area and pore volume as the non-promoted catalyst, indicating that the small quantities of Co did not have a significant effect on the textural properties of the catalysts. Also, Table 1 shows that pore volume decreases slightly with Cu and Co deposition, suggesting that there was no significant pore mouth blockage.

Figure 1 shows the XRD patterns of the Cu/Al<sub>2</sub>O<sub>3</sub> and Co(y)Cu/Al<sub>2</sub>O<sub>3</sub> catalysts.

**Table 1:** Textural properties and metal contents of Cu/Al<sub>2</sub>O<sub>3</sub> and Co(y)Cu/Al<sub>2</sub>O<sub>3</sub> catalyst samples

Samples	Metal Content (wt.%) <sup>*</sup>		$S_{BET}$ (m <sup>2</sup> g <sup>-1</sup> )	Vp (cm <sup>3</sup> g <sup>-1</sup> )
	Cu	Co		
Al <sub>2</sub> O <sub>3</sub>			319	0.35
Cu/Al <sub>2</sub> O <sub>3</sub>			229	0.31
Co(0.8)Cu/Al <sub>2</sub> O <sub>3</sub>	7.8	0.8	225	0.31
Co(1.0)Cu/Al <sub>2</sub> O <sub>3</sub>	7.6	1.0	227	0.33
Co(1.3)Cu/Al <sub>2</sub> O <sub>3</sub>	7.2	1.3	215	0.31
Co(1.5)Cu/Al <sub>2</sub> O <sub>3</sub>	6.7	1.5	213	0.31

<sup>\*</sup>Real Cu and Co content obtained from ICP analysis



**Figure 1.** X-ray diffraction patterns for calcined of the Cu/Al<sub>2</sub>O<sub>3</sub> and Co(y)Cu/Al<sub>2</sub>O<sub>3</sub> catalysts

Characteristic diffraction peaks of CuO at  $2\theta = 35.0^\circ$  and  $39.0^\circ$  were detected, assigned to base-centered monoclinic phase (JCPDS PDF: 48-1548), and for  $\gamma$ -Al<sub>2</sub>O<sub>3</sub> at  $2\theta = 37.6^\circ$ ,  $45.7^\circ$  and  $67.0^\circ$  (JSPDS PDF: 10-0425) were observed<sup>35-37</sup>. Other species such as spinel CuAl<sub>2</sub>O<sub>4</sub>, which is typically formed after calcination at 400 °C, or CuCo<sub>2</sub>O<sub>4</sub> which is usually formed after calcination below 300 °C<sup>38</sup>, were not identified. However, Lee *et al.*<sup>39</sup> have reported that diffraction peaks of CuCo<sub>2</sub>O<sub>4</sub> nanoparticles appear at  $2\theta = 19.0^\circ$ ,  $37.0^\circ$  and  $38.7^\circ$ , corresponding to (111) (311) and (222) planes, respectively. Thus, the absence of these peaks could be due to the formation of highly-dispersed species, or the masking of diffraction peaks by broad peaks of the  $\gamma$ -Al<sub>2</sub>O<sub>3</sub> support. Therefore, to further understand the effect of Co addition on the structure of supported Cu catalysts, quantitative phase analysis by Rietveld refinement was carried out (the results are summarized in Table 2). From the experimental analysis, some sharp peaks appeared to be superimposed on top of the smooth pattern of the nano-crystalline  $\gamma$ -alumina support. There were no sharp peaks observed on the other end of the diffraction angle. However, the pattern obtained after subtraction of the pattern of the  $\gamma$ -Al<sub>2</sub>O<sub>3</sub> support from that of the sample could tentatively be identified as a spinel structure, such as CuCo<sub>2</sub>O<sub>4</sub>. Therefore, the CuCo<sub>2</sub>O<sub>4</sub> structure was modelled using the structure reported by Wyckoff<sup>40</sup>. Table 2 shows that the fraction CuCo<sub>2</sub>O<sub>4</sub> increased as the concentration of Co increased in the samples. The overall trends can be seen in Figure 2. Thus, based on Rietveld analysis, the addition of Co to Cu/Al<sub>2</sub>O<sub>3</sub> created a new phase (CuCo<sub>2</sub>O<sub>4</sub>) whose relative fraction increased with Co content. It is assumed that this new phase probably improved the surface distribution and stability of Cu species in the promoted catalyst.

**Table 2.** Rietveld refinement results (relative phase fractions) for samples of different Co content (wt %)

Co	0.8%	1.0%	1.3%	1.5%
Sigma	1.276	1.273	1.231	1.241
Rwp %	3.081	2.947	2.936	2.911
intensity	788	771	784	719
Al <sub>2</sub> O <sub>3</sub>	99.960	99.436	99.591	99.459
CuCo <sub>2</sub> O <sub>4</sub>	0.040	0.329	0.409	0.541

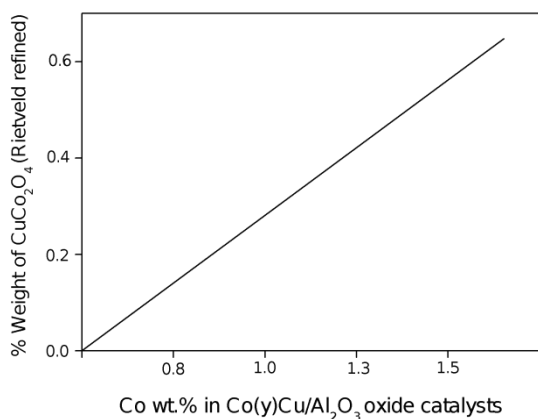


**Figure 2.** Rietveld refined from experimental X-ray diffraction calculation for Co(y)Cu/Al<sub>2</sub>O<sub>3</sub> catalyst

Figure 3 shows the H<sub>2</sub>-TPR profiles of the catalysts. The reducibility of the catalysts provides useful information on the species present on the surface of the catalyst and insights into the nature of the active sites, particularly since it is assumed that *in-situ* reduction occurred during glycerol hydrogenolysis reaction at 220 °C. The TPR profile of Cu/Al<sub>2</sub>O<sub>3</sub> presented one main peak at 200 °C, assigned to the reduction of highly dispersed CuO species to Cu<sup>0</sup><sup>41, 42</sup>; furthermore, a shoulder appears at 240 °C which is attributed to the reduction of Cu<sup>+</sup> to Cu<sup>0</sup><sup>43, 44</sup>, or to the reduction of larger particles of Cu<sup>2+</sup> to Cu<sup>0</sup><sup>43</sup>. The TPR profile of a reference Co(1.5%)/Al<sub>2</sub>O<sub>3</sub> sample presented a low-intense peak at 280 °C, assigned to the reduction of Co<sup>2+</sup> to Co<sup>0</sup><sup>45-47</sup>. There was no evidence of the step-wise reduction of cobalt oxide (Co<sub>3</sub>O<sub>4</sub> → CoO → Co<sup>0</sup>) that is commonly observed for catalysts with high Co content ( $\geq 10$  wt.%)<sup>45, 46</sup>. For the Co(y)Cu/Al<sub>2</sub>O<sub>3</sub> catalysts, the reduction peaks associated with Cu species were the most prominent while those corresponding to Co species were not visible. The absence of the reduction peak for Co species may be due to an overlap with the reduction signals of Cu<sup>2+</sup> species, suggesting that Cu promoted the reduction of CoO species. Kaluza *et al.*<sup>48</sup> reported that during reduction of supported Co-Cu catalysts, adsorbed atomic hydrogen could migrated from Cu<sup>0</sup> to Co oxide species and promote reduction to Co<sup>0</sup> via a possible spillover mechanism. The reduction profile of the Co(1.5)Cu/Al<sub>2</sub>O<sub>3</sub> catalyst shows a weak but obvious feature around 325 °C. This may be linked to the reduction of CuCo<sub>2</sub>O<sub>4</sub>, as suggested by XRD results. The profiles of the Co(y)Cu/Al<sub>2</sub>O<sub>3</sub> catalysts show a weak feature around 750 °C, attributed to the reduction of aluminates species (CuAl<sub>2</sub>O<sub>4</sub>).

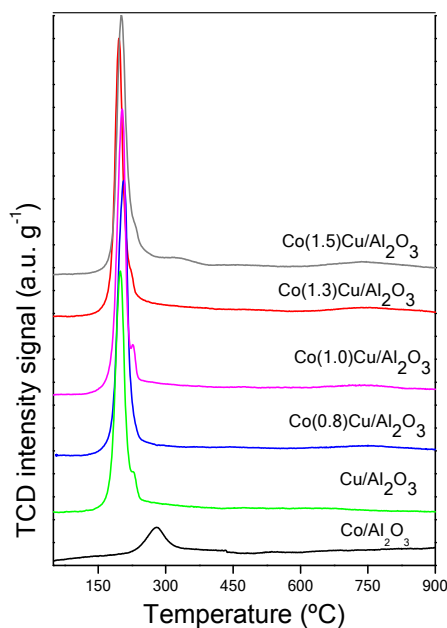


**Figure 3.** H<sub>2</sub>-TPR of Co/Al<sub>2</sub>O<sub>3</sub>, Cu/Al<sub>2</sub>O<sub>3</sub> and Co(y)Cu/Al<sub>2</sub>O<sub>3</sub> catalysts

Table 3 lists XPS results of reduced catalysts. The analysis provides complementary information on the presence of cobalt and/or Cu aluminates species as well as gives insight into the stability of the oxides. The binding energy (BE) of Cu 2p<sub>3/2</sub> is observed at  $932.7 \pm 0.1$  (eV), attributed to Cu<sup>0</sup> species<sup>49-51</sup>. Based on  $\Delta A$  parameter from XPS measurements, a signal at  $1851.1 \pm 0.1$  (eV) was detected, indicating only Cu<sup>0</sup> species is distinguished on the surface of the catalysts, in agreement with conclusion drawn by

previous work<sup>52</sup>. This result suggests a complete reduction of Cu species under the experimental condition used. The Co 2p<sub>3/2</sub> signal revealed a doublet with BE at 778.0 ± 0.1 and 780.1 ± 0.1 (eV), assigned typically to Co<sup>0</sup> and Co<sup>2+</sup> species, respectively<sup>47, 53</sup>. However, other studies related to CuCo<sub>2</sub>O<sub>4</sub> nanocrystals and spinel structures have reported that the BE at 780.0 eV is associated with the presence of Co<sup>3+</sup><sup>54-56</sup>.

Therefore, the co-existence of Co<sup>2+</sup> surface species and Co<sup>3+</sup> associated to CuCo<sub>2</sub>O<sub>4</sub> structures cannot be ruled out. Table 3 also shows that the fraction of Co species in metallic state increased with Co loading from 0.8 to 1.3 wt.%, and then decreased at a higher loading. This indicates that Co becomes easier to reduce due to weaker Co-Cu interaction as Co content increases, as suggested by TPR results. In fact, Medina *et al.*<sup>47</sup> proposed that at low Co content, Co<sup>2+</sup> species interact strongly with the support, hindering complete reduction to metallic Co. Conversely, larger, more-easily reducible particles are formed at higher Co loadings. No shifts in binding energies were observed, indicating the absence of charge transfer. This is reasonable due to the marginal difference of electronegativity values between Cu (1.90) and Co (1.88).

For this reason, it appears that an ensemble effect was

Oxide catalysts	Al2p (eV)	Cu2p <sub>3/2</sub> (eV)	Co2p <sub>3/2</sub> (eV)	O1s (eV)	Cu/Al	Co/Al
Cu/Al <sub>2</sub> O <sub>3</sub>		932.7	--		0.021	
Co(0.8)Cu/Al <sub>2</sub> O <sub>3</sub>	74.5	932.8	778.0 (61) 780.1 (39)	531.4	0.060	0.024
Co(1.0)Cu/Al <sub>2</sub> O <sub>3</sub>	74.5	932.7	778.1 (66) 780.1 (34)	531.4	0.058	0.041
Co(1.3)Cu/Al <sub>2</sub> O <sub>3</sub>	74.5	932.7	778.0 (72) 780.1 (28)	531.5	0.064	0.054
Co(1.5)Cu/Al <sub>2</sub> O <sub>3</sub>	74.5	932.8	778.1 (68) 780.1 (32)	531.5	0.063	0.060

operational upon the addition of Co to Cu/Al<sub>2</sub>O<sub>3</sub>, consistent with UV-DRS results which showed changes to the coordination symmetry and geometry of copper oxide species. Figure 4 shows an increase in the Co/Al atomic ratio, while the Cu/Al atomic ratio remained almost unchanged. This is consistent with the loadings and indicates that Co and Cu species are well dispersed on the surface and in the bulk of the catalysts.

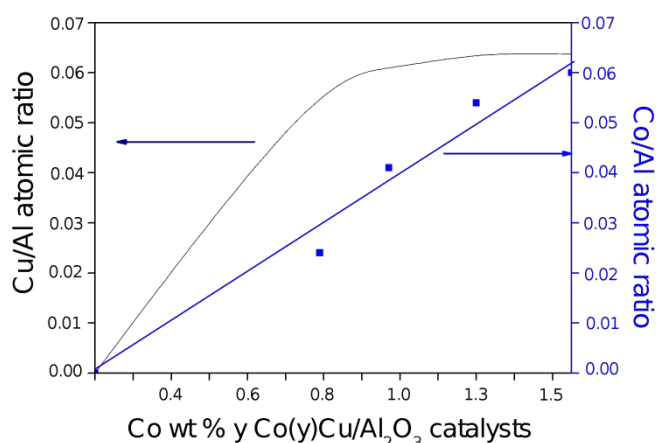


**Figure 4.** Co/Al and Cu/Al atomic ratio obtained from XPS measurements for Cu/Al<sub>2</sub>O<sub>3</sub> and Co(y)Cu/Al<sub>2</sub>O<sub>3</sub> catalysts

Figure S1 (supplementary information) shows the UV-DRS spectra of Cu/Al<sub>2</sub>O<sub>3</sub> and Co(y)Cu/Al<sub>2</sub>O<sub>3</sub> oxide catalysts. This was

performed in order to analyze the effect of the presence of Co on the coordination symmetry of Cu oxide species. Figure S1 shows that the main bands observed are between 350 and 450 nm which is associated with the octahedral geometry (hexacoordinated symmetry) of Cu<sup>2+</sup> species<sup>57-59</sup>. Other bands observed between 600-900 nm are attributed to d-d electronic transition of Cu<sup>2+</sup> corresponding to the distorted octahedral geometry (pentacoordinated symmetry)<sup>57-59</sup>. In order to determine the effect of Co oxide species on the symmetry of CuO species, the ratio of the intensities (IOh/IOhD) between octahedral Cu<sup>2+</sup> species (IOh) and octahedral distorted Cu<sup>2+</sup> species (IOhD) as a function of Co content was calculated (Figure 5). It can be observed that the (IOh/IOhD) ratio decreased after Co addition, reaching a minimum value at 1.0 wt.% of Co, and then increased at higher Co content. The decrease of (IOh/IOhD) ratio suggests a distortion of octahedral symmetry of CuO species by the presence of Co oxide, probably due to a CoOx-CuOx interaction. This behavior agrees with previous results by Xiao *et al.*<sup>60</sup>, in which a partial substitution or insertion of CoO in Cu octahedral oxide structure was proposed to have occurred. This behavior was also similarly observed by Wang *et al.*<sup>61</sup> for Co-Ce oxide catalysts.

In contrast, the increase of (IOh/IOhD) ratio observed at higher Co content could be attributed to a decrease in the interaction between CoOx and CuOx species. Another possible reason could be inferred from XRD quantitative phase analysis results.

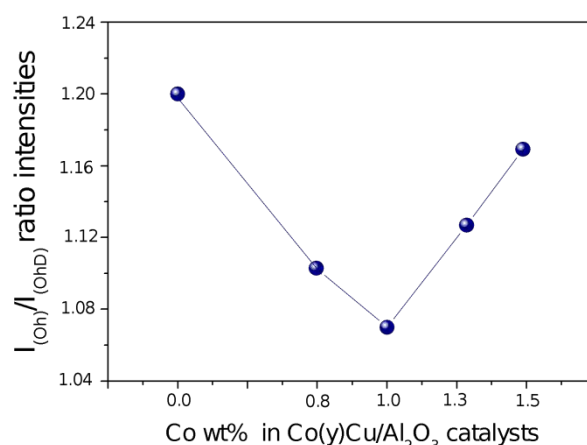


**Figure 5.** (IOh/IOhD) ratio of octahedral Cu<sup>2+</sup> species (IOh) and octahedral distorted Cu<sup>2+</sup> species (IOhD) as a function of Co content for Cu/Al<sub>2</sub>O<sub>3</sub> and Co(y)Cu/Al<sub>2</sub>O<sub>3</sub> catalysts

Figure 6 shows the TPD-NH<sub>3</sub> profiles of Cu/Al<sub>2</sub>O<sub>3</sub> and Co(y)Cu/Al<sub>2</sub>O<sub>3</sub> oxide catalysts. After deconvolution of the desorption profile with a Gaussian function, acid sites distribution was calculated from areas spanning different ranges of temperature: weak acid sites (<300 °C), medium acid sites (between 300 and 500 °C) and strong acid sites (> 500 °C)<sup>31</sup>. Figure 6 shows that, except for Co(1.5)Cu/Al<sub>2</sub>O<sub>3</sub>, the addition of Co significantly

increased the intensity of NH<sub>3</sub> desorption peaks in comparison to Cu/Al<sub>2</sub>O<sub>3</sub>.

Interestingly, the intensity of the desorption signals decreased after further increase of Co content above 1.0 wt%. Table 4 gives quantitative evidence of the effect of variable Co loading on acidity. Total amount of acid sites increases with Co loading, goes through a maximum at a nominal Co content of 1.0 wt%, and decreases at higher loadings. The increase in total acid sites is probably related to the presence of adjacent Co<sup>2+</sup> sites through the formation of CuCo<sub>2</sub>O<sub>4</sub>. In contrast, the decrease of total acid sites at higher Co content could be linked to formation of less-acidic aluminates (CoCuAl<sub>2</sub>O<sub>3</sub>). This is most evident on the catalyst with the highest Co content (Co(1.5)Cu/Al<sub>2</sub>O<sub>3</sub>), in which a drastic decrease in total amount of total acid sites could be related to the presence of CoCuAl<sub>2</sub>O<sub>3</sub> species, as deduced from TPR result.

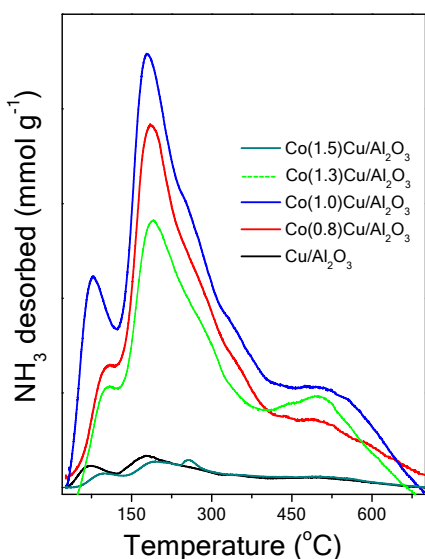


Figure 6 TPD-NH<sub>3</sub> profiles of Cu/Al<sub>2</sub>O<sub>3</sub> and Co(y)Cu/Al<sub>2</sub>O<sub>3</sub> catalysts

Regardless of the change in the total amount of acid sites, it can be estimated from Table 4 that weak acid sites account for 55-68 % of the total acid sites. Thus, weak acid sites are mainly responsible for any acid-catalysed reactions during the hydrogenolysis of glycerol.

**Table 4** Total acidity and acid sites distribution on calcined Cu/Al<sub>2</sub>O<sub>3</sub> and Co(y)Cu/Al<sub>2</sub>O<sub>3</sub> catalysts (x10<sup>-4</sup>mol NH<sub>3</sub> g<sup>-1</sup>)

Catalysts	Weak	Medium	Strong	Total
Cu/Al <sub>2</sub> O <sub>3</sub>	0.97	0.29	0.18	1.4
Co/Al <sub>2</sub> O <sub>3</sub>	4.50	9.38	3.22	17.1
Co(0.8)Cu/Al <sub>2</sub> O <sub>3</sub>	7.79	2.54	1.07	11.4
Co(1.0)Cu/Al <sub>2</sub> O <sub>3</sub>	9.73	5.14	2.23	17.1
Co(1.3)Cu/Al <sub>2</sub> O <sub>3</sub>	7.88	2.82	1.69	12.4
Co(1.5)Cu/Al <sub>2</sub> O <sub>3</sub>	0.69	0.37	0.20	1.3

the total acid sites. Thus, weak acid sites are mainly responsible for any acid-catalysed reactions during the hydrogenolysis of glycerol.

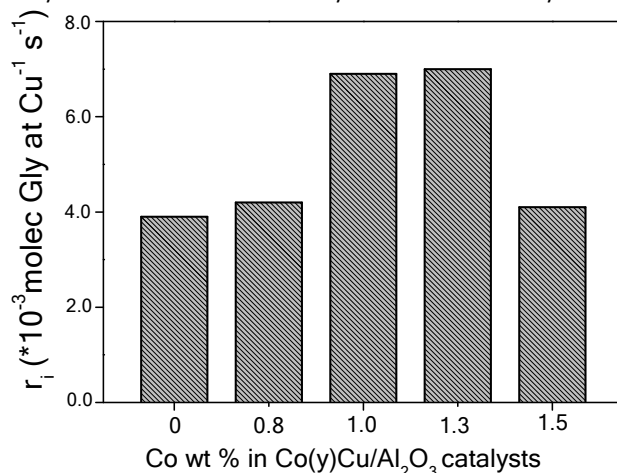
## 2.2 Catalytic activity of CuO/Al<sub>2</sub>O<sub>3</sub> and Co(x)Cu/Al<sub>2</sub>O<sub>3</sub> catalysts

Hydrogenolysis of glycerol over Cu-based catalysts have been reported in the literature<sup>7, 9, 12, 19, 33</sup> and it proceeds through two principal routes: (i) C-C bond breaking, in which glycerol is converted to ethyleneglycol, and subsequently to methanol by hydrogenation; and (ii) C-O bond cleavage (dehydration of glycerol) to form hydroxyacetone (acetol) and 3-hydroxypropanal (3-HPA) as intermediates, which are then further hydrogenated to form 1,2-PDO and 1,3-PDO, respectively (1,2-PDO and 1,3-PDO can undergo additional hydrogenation to produced propanols). The intermediate product, 3-hydroxypropanal, can also be dehydrated to 2-propenal (acrolein) and propanoic acid<sup>1, 19, 33</sup>, as shown in Scheme 1. Table 5 summarizes the catalytic activity of the Cu/Al<sub>2</sub>O<sub>3</sub> and Co(y)Cu/Al<sub>2</sub>O<sub>3</sub> oxide catalysts, represented by initial intrinsic rate (expressed as molecule of glycerol converted per atom of Cu per time). Figure 7 illustrates the result.

**Table 5.** Catalytic activity and selectivity of Cu/Al<sub>2</sub>O<sub>3</sub> and Co(y)Cu/Al<sub>2</sub>O<sub>3</sub> catalysts in hydrogenolysis of glycerol at 220 °C and 5 MPa H<sub>2</sub>

Catalysts	Intrinsic rate (* 10 <sup>-3</sup> molec gly Cu at <sup>-1</sup> s <sup>-1</sup> )	Selectivity (calculated at 10 % of glycerol conversion)					
		1,2-PDO	acetol	1-P	Ethy	PA	oths
Cu/Al <sub>2</sub> O <sub>3</sub>	3.9	65	20	6.5	--	--	8.5
Co(0.8)Cu/Al <sub>2</sub> O <sub>3</sub>	4.2	79	15	6.0	--	--	--
Co(1.0)Cu/Al <sub>2</sub> O <sub>3</sub>	6.9	61	24	5.0	--	2.0	8.0
Co(1.3)Cu/Al <sub>2</sub> O <sub>3</sub>	7.0	78	19	1.0	2.0	--	--
Co(1.5)Cu/Al <sub>2</sub> O <sub>3</sub>	4.1	87	12	1.0	--	--	--

The addition of Co increased the catalytic activity, reached a maximum with Co content of 1.0 and 1.3 wt.%, and then decreased at a higher Co loading. The increase in activity could be explained by two complementary effects. The effect is related to the presence of CuCo<sub>2</sub>O<sub>4</sub> species, as obtained from Rietveld refinement of XRD patterns. The formation of CuCo<sub>2</sub>O<sub>4</sub> species is alluded to as the reason for the highest amount of acid sites on the Co(1.0)Cu/Al<sub>2</sub>O<sub>3</sub> catalyst. This increase of acidity could favour dehydration of



glycerol to acetol. The second effect is related to changes of coordination symmetry and geometry of the copper oxide species observed by DRS-UV. The presence of multiple adjacent Co sites on

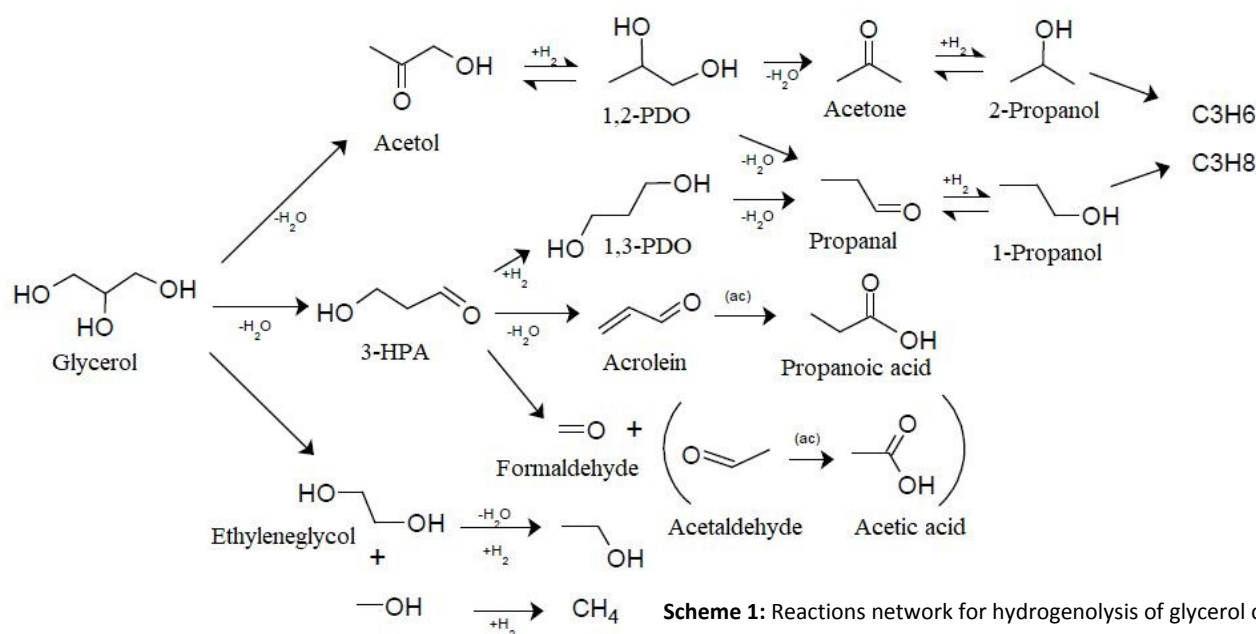
the surface of Cu/Al<sub>2</sub>O<sub>3</sub> (as deduced from XPS results) could favour the hydrogenation step, specifically to the formation of 1,2-PDO.

presence of acid sites, probably associated with Co<sup>2+</sup> and XRD quantitative analysis reveal the existence of mixed oxides (CuCo<sub>2</sub>O<sub>4</sub>).

**Figure 7.** Catalytic activity as a function of Co content on Co(y)Cu/Al<sub>2</sub>O<sub>3</sub> catalysts

In general, the yields of products over all the catalysts were similar. It can be observed that hydrogenolysis of glycerol led to 1,2-PDO as the principal product, acetol as an intermediate product, and 2-propanol (2-P) as a minor product. Other products observed in trace amounts include propanoic acid (PA), 1,3-PDO, acetic acid, propanal and ethylene glycol (Ethy). But, selectivity calculated at a glycerol conversion of 10%, present differences after Co oxide addition on the Cu/Al<sub>2</sub>O<sub>3</sub> catalysts, which

Although the surface concentration of these sites differs depending on Co content, the nature of the sites remains largely unaffected. This is probably one of the reasons why product selectivity did not vary substantially with Co content. Another reason could be the relative activity of the multiple sites that participate in the transformation of glycerol. It is not yet clear whether the coexistence of these sites promotes or hinders each other. For example, metallic Co and Cu are both hydrogenation sites but Cu/Al<sub>2</sub>O<sub>3</sub> and Co(1.0)Cu/Al<sub>2</sub>O<sub>3</sub> have similar selectivity towards 1,2-PDO formation. Therefore, it is not certain whether these sites are beneficial to the formation of 1,2-PDO. Another example is the role of acidity on acetol formation, an intermediate to 1,2-PDO. Kinetic and spectroscopic analysis of individual pathways are on-going to shed more insight into the role of these sites on the main reaction routes.



are evidenced in Figure 8 and Table 5. Selectivity to 1,2-PDO ranges from 61-87%, and the selectivity to acetol ranges from 12-24%, indicating that Co(y)Cu/Al<sub>2</sub>O<sub>3</sub> catalysts significantly favor the consecutive C-O bond cleavage and hydrogenation pathway over the other pathways. Figure 8 shows that no clear trend can be observed with Co content. This is not unexpected because the main products are formed sequentially. According to previous studies, the initial transformation of glycerol to acetol is catalyzed by acid sites, while

the subsequent hydrogenation to 1,2-PDO is catalyzed by active metallic sites<sup>19, 33, 62, 63</sup>. Characterization results indicate the presence of these sites on the Co(y)Cu/Al<sub>2</sub>O<sub>3</sub> catalysts. XPS results indicate the presence of metallic Cu and Co, UV-DRS and TPR results hint at adjacent Cu and Co atoms, TPD-NH<sub>3</sub> results show the

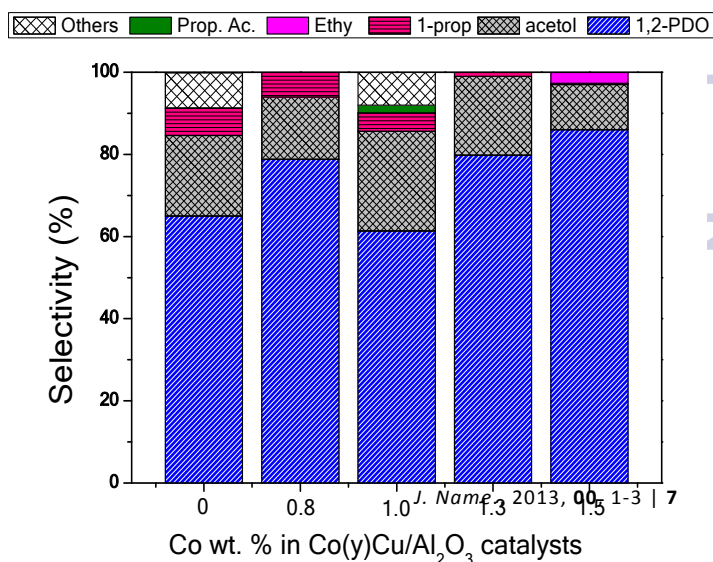


**Figure 8.** Product distribution calculated at 10% conversion of glycerol on Cu/Al<sub>2</sub>O<sub>3</sub> and Co(y)Cu/Al<sub>2</sub>O<sub>3</sub> catalysts

## Conclusions

This study showed two main effects. First, alumina-supported Cu catalysts are active for the hydrogenolysis of glycerol. Second, the addition of CoO to CuO/Al<sub>2</sub>O<sub>3</sub> had a beneficial effect on catalytic activity. However, the effect of Co loading on activity was parabolic. Characterization results show that the addition of appropriate amount of Co to Cu/Al<sub>2</sub>O<sub>3</sub> leads to the formation of adjacent Co and Cu atoms, increase in the number acid sites, and formation of mixed oxides (CuCo<sub>2</sub>O<sub>4</sub>), leading to enhanced activity. On the other hand, a high Co loading (1.5 wt.%) decreases acidity and promotes the formation of aluminates (CoCuAl<sub>2</sub>O<sub>3</sub>), leading to diminished activity. All the catalysts exhibited a substantial preference for C-O hydrogenolysis to acetol and the subsequent hydrogenation to 1,2-PDO due to presence of metallic and acidic sites. The lack of consistent trend of product selectivity as a function of Co loading is linked to the existence of the same type of active sites on the catalysts, regardless of Co content.

## Conflicts of interest

There are no conflicts to declare

## Acknowledgements

The authors thank CONICYT-Chile for FONDECYT N° 11130376. The authors also gratefully acknowledge the financial support under CONICYT PIA CTE AFB170007, FONDEQUIP EQM 120096 and 150103 grants. This work was also supported by funding from Millennium Science Initiative of the Ministry of Economy, Development and Tourism, Nuclei on Catalytic Processes towards Sustainable Chemistry (CSC) grant.

## References

- I. Gandarias, P. L. Arias, J. Requies, M. B. Güemez and J. L. G. Fierro, *Applied Catalysis B: Environmental*, 2010, **97**, 248-256.
- C.-H. Zhou, J. N. Beltramini, Y.-X. Fan and G. Q. Lu, *Chem. Soc. Rev.*, 2008, **37**, 527-549.
- R. Ciriminna, C. D. Pina, M. Rossi and M. Pagliaro, *Eur. J. Lipid Sci. Technol.*, 2014, **116**, 1432-1439. DOI: 10.1039/C9NJ03534F
- M. Pagliaro, R. Ciriminna, H. Kimura, M. Rossi and C. Della Pina, *Angew. Chem., Int. Ed. Engl.*, 2007, **46**, 4434-4440.
- A. Seretis and P. Tsiakaras, *Fuel Process. Technol.*, 2015, **134**, 107-115.
- X. Guo, Y. Li, R. Shi, Q. Liu, E. Zhan and W. Shen, *Appl. Catal., A*, 2009, **371**, 108-113.
- A. Bienholz, H. Hofmann and P. Claus, *Appl. Catal., A*, 2011, **391**, 153-157.
- S. S. Priya, V. P. Kumar, M. L. Kantam, S. K. Bhargava, S. Periasamy and K. V. R. Chary, *Appl. Catal., A*, 2015, **498**, 88-98.
- Z. Huang, F. Cui, J. Xue, J. Zuo, J. Chen and C. Xia, *Catal. Today*, 2012, **183**, 42-51.
- Y. Kusunoki, T. Miyazawa, K. Kunimori and K. Tomishige, *Catal. Commun.*, 2005, **6**, 645-649.
- C. Sepúlveda, L. Delgado, R. García, M. Melendrez, J. L. G. Fierro, I. T. Ghampson and N. Escalona, *Catal. Today*, 2017, **279**, Part 2, 217-223.
- E. S. Vasiliadou, T. M. Eggenhuisen, P. Munnik, P. E. de Jongh, K. P. de Jong and A. A. Lemonidou, *Appl. Catal., B*, 2014, **145**, 108-119.
- A. Kant, Y. He, A. Jawad, X. Li, F. Rezaei, J. D. Smith and A. A. Rownaghi, *Chem. Eng. J.*, 2017, **317**, 1-8.
- R. J. Chimentão, B. C. Miranda, J. Szanyi, C. Sepulveda, J. B. O. Santos, J. V. S. Correa, J. Llorca and F. Medina, *Molecular Catalysis*, 2017, **435**, 49-57.
- B. C. Miranda, R. J. Chimentão, J. B. O. Santos, F. Gispert-Guirado, J. Llorca, F. Medina, F. L. Bonillo and J. E. Sueiras, *Appl. Catal., B*, 2014, **147**, 464-480.
- P. Khemthong, W. Klysubun, S. Prayoonpokarach, F. Roessner and J. Wittayakun, *Journal of Industrial and Engineering Chemistry*, 2010, **16**, 531-538.
- X. Guo, Y. Li, R. Shi, Q. Liu, E. Zhan and W. Shen, *Appl. Catal., A*, 2009, **371**, 108-113.
- L. Li, D. Mao, J. Yu and X. Guo, *J. Power Sources*, 2015, **279**, 394-404.
- R. V. Sharma, P. Kumar and A. K. Dalai, *Appl. Catal., A*, 2014, **477**, 147-156.
- Mzamo L. Shoji, V. D. B. C. Dasireddy, S. Singh, A. Govender, P. Mohlala and H. B. Friedrich, *Sustainable Energy & Fuels*, 2019, **3**, 2038-2047.
- M. L. Shoji, V. D. B. C. Dasireddy, S. Singh, P. Mohlala, D. J. Morgan, S. Iqbal and H. B. Friedrich, *Sustainable Energy & Fuels*, 2017, **1**, 1437-1445.
- M. L. Shoji, V. D. B. C. Dasireddy, S. Singh, P. Mohlala, D. J. Morgan and H. B. Friedrich, *ACS Sustainable Chemistry & Engineering*, 2016, **4**, 5752-5760.
- Y. Wang, Y. Zheng, Y. Wang, K. Li, Y. Wang, L. Jiang, X. Zhu, Y. Wei and H. Wang, *Appl. Surf. Sci.*, 2019, DOI: <https://doi.org/10.1016/j.apsusc.2019.03.050>.
- A. Martínez-Arias, A. B. Hungría, G. Munuera and D. Gamarra, *Appl. Catal., B*, 2006, **65**, 207-216.
- S. Zhang and Y. Guo, *Chem. Phys. Lett.*, 2019, **722**, 26-31.
- M. L. Hernández, J. A. Montoya, I. Hernández, M. Viniegra, M. E. Llanos, V. Garibay and P. D. Angel, *Microporous Mesoporous Mater.*, 2006, **89**, 186-195.
- C.-L. Chiang and K.-S. Lin, *Int. J. Hydrogen Energy*, 2017, **42**, 23526-23538.
- L. Li, D. Mao, J. Xiao, L. Li, X. Guo and J. Yu, *Chem. Eng. Res. Des.*, 2016, **111**, 100-108.

29. A. Amri, Z.-T. Jiang, N. Wyatt, C.-Y. Yin, N. Mondinos, T. Pryor and M. M. Rahman, *Ceram. Int.*, 2014, **40**, 16569-16575.
30. H. M. Rietveld, *J. Appl. Crystallogr.*, 1969, **2**, 65-71.
31. R. Nava, B. Pawelec, P. Castaño, M. C. Álvarez-Galván, C. V. Loricera and J. L. G. Fierro, *Applied Catalysis B: Environmental*, 2009, **92**, 154-167.
32. A. López, J. A. Aragón, J. G. Hernández-Cortez, M. L. Mosqueira and R. Martínez-Palou, *Molecular Catalysis*, 2019, **468**, 9-18.
33. F. Vila, M. López Granados, M. Ojeda, J. L. G. Fierro and R. Mariscal, *Catal. Today*, 2012, **187**, 122-128.
34. T. Sánchez, P. Salagre, Y. Cesteros and A. Bueno-López, *Chem. Eng. J.*, 2012, **179**, 302-311.
35. I. Gandarias, J. Reques, P. L. Arias, U. Armbruster and A. Martin, *J. Catal.*, 2012, **290**, 79-89.
36. T.-W. Kim, M.-W. Song, H.-L. Koh and K.-L. Kim, *Appl. Catal., A*, 2001, **210**, 35-44.
37. R. Valencia, J. A. Tirado, R. Sotelo, F. Trejo and L. Lartundo, *Reaction Kinetics, Mechanisms and Catalysis*, 2015, **116**, 205-222.
38. M. Wojciechowska, M. Zieliński, A. Malczewska, W. Przystajko and M. Pietrowski, *Appl. Catal., A*, 2006, **298**, 225-231.
39. A. K. Das, N. H. Kim, S. H. Lee, Y. Sohn and J. H. Lee, *Composites Part B: Engineering*, 2018, **150**, 269-276.
40. *Journal*.
41. K. V. R. Chary, K. K. Seela, G. V. Sagar and B. Sreedhar, *J. Phys. Chem. B*, 2004, **108**, 658-663.
42. A. J. Marchi, J. L. G. Fierro, J. Santamaría and A. Monzón, *Appl. Catal., A*, 1996, **142**, 375-386.
43. L.-F. Chen, P.-J. Guo, M.-H. Qiao, S.-R. Yan, H.-X. Li, W. Shen, H.-L. Xu and K.-N. Fan, *J. Catal.*, 2008, **257**, 172-180.
44. M. L. Smith, A. Campos and J. J. Spivey, *Catalysis Today*, 2012, **182**, 60-66.
45. W.-J. Wang and Y.-W. Chen, *Appl. Catal.*, 1991, **77**, 223-233.
46. Y. Liu, L. Jia, B. Hou, D. Sun and D. Li, *Appl. Catal., A*, 2017, **530**, 30-36.
47. C. Medina, R. García, P. Reyes, J. L. G. Fierro and N. Escalona, *Appl. Catal., A*, 2010, **373**, 71-75.
48. J. Anton, J. Nebel, H. Song, C. Froese, P. Weide, H. Ruland, M. Muhler and S. Kaluza, *Appl. Catal., A*, 2015, **505**, 326-333.
49. F. E. López-Suárez, A. Bueno-López and M. J. Illán-Gómez, *Appl. Catal., B*, 2008, **84**, 651-658.
50. J. Agrell, H. Birgersson, M. Boutonnet, I. Melián-Cabrera, R. M. Navarro and J. L. G. Fierro, *J. Catal.*, 2003, **219**, 389-403.
51. G. G. Jernigan and G. A. Somorjai, *J. Catal.*, 1994, **147**, 567-577.
52. D. Sun, Y. Yamada, S. Sato and W. Ueda, *Applied Catalysis B: Environmental*, 2016, **193**, 75-92.
53. W. Zhou, J.-G. Chen, K.-G. Fang and Y.-H. Sun, *Fuel Process. Technol.*, 2006, **87**, 609-616.
54. Y. Zhao, X. Zhou, Y. Ding, J. Huang, M. Zheng and W. Ye, *J. Catal.*, 2016, **338**, 30-37.
55. Y. Zhao, J. Lin, Y. Liu, B. Ma, Y. Ding and M. Chen, *Chem. Commun. (Cambridge, U. K.)*, 2015, **51**, 17309-17312.
56. P. Li, W. Sun, Q. Yu, P. Yang, J. Qiao, Z. Wang, D. Rooney and K. Sun, *Solid State Ionics*, 2016, **289**, 17-22.
57. R. Hierl, H. Knözinger and H.-P. Urbach, *J. Catal.*, 1981, **69**, 475-486.  
DOI: 10.1039/C9NJ03534F
58. H. Praliaud, S. Mikhailenko, Z. Chajar and M. Primet, *Appl. Catal., B*, 1998, **16**, 359-374.
59. B. R. Strohmeier, D. E. Levden, R. S. Field and D. M. Hercules, *J. Catal.*, 1985, **94**, 514-530.
60. Y. Wang, Y. Miao, S. Li, L. Gao and G. Xiao, *Molecular Catalysis*, 2017, **436**, 128-137.
61. C. Wang, C. Zhang, W. Hua, Y. Guo, G. Lu, S. Gil and A. Giroir-Fendler, *Chem. Eng. J.*, 2017, **315**, 392-402.
62. C. Montassier, D. Giraud and J. Barbier, in *Stud. Surf. Sci. Catal.*, eds. M. Guisnet, J. Barrault, C. Bouchoule, D. Duprez, C. Montassier and G. Pérot, Elsevier, 1988, vol. 41, pp. 165-170.
63. M. A. Dasari, P.-P. Kiatsimkul, W. R. Sutterlin and G. J. Suppes, *Appl. Catal., A*, 2005, **281**, 225-231.

## Table of contents

View Article Online  
DOI: 10.1039/C9NJ03534F

The  $\text{CuCo}_2\text{O}_4$  species formed by  $\text{CoO}$  addition on  $\text{CuO}/\text{Al}_2\text{O}_3$  had a beneficial effect on catalytic activity in hydrogenolysis of glycerol

